

Contribution to the 13th International Conference on the Physics of Non-Ideal Plasmas  
(PNP 13), 13-18 September 2009, Chernogolovka

## Laser Acoustic Probing of Two-Temperature Zone Created by Femtosecond Pulse

N. A. Inogamov<sup>\*1</sup>, V. V. Zhakhovsky<sup>2,3</sup>, S. I. Ashitkov<sup>2</sup>, V. A. Khokhlov<sup>1</sup>, V. V. Shepelev<sup>4</sup>, P. S. Komarov<sup>2</sup>, A. V. Ovchinnikov<sup>2</sup>, D. S. Sitnikov<sup>2</sup>, Yu. V. Petrov<sup>1</sup>, M. B. Agranat<sup>2</sup>, S. I. Anisimov<sup>1</sup>, and V. E. Fortov<sup>2</sup>

<sup>1</sup> Landau Institute for Theoretical Physics, Russian Academy of Sciences, Chernogolovka 142432, Russia

<sup>2</sup> Joint Institute for High Temperatures, Russian Academy of Sciences, Moscow 125412, Russia

<sup>3</sup> University of South Florida, Department of Physics, Tampa, Florida 33620, USA

<sup>4</sup> Institute for Computer Aided Design, Russian Academy of Sciences, Moscow 123056, Moscow, Russia

Received 11 September 2009, accepted 15 December 2009

Published online 4 May 2010

**Key words** Two-temperature warm dense matter, action of ultrashort laser pulse, pump-probe technique.

We combine theoretical and experimental methods to study the processes induced by fast laser heating of metal foils. These processes reveal themselves through motion of frontal (irradiated) and rear-side foil boundaries. The irradiated targets are 0.3-2 micron thick aluminum foils deposited on much thicker (150 microns) glass plate. The instant boundary positions is measured by pump-probe technique having  $\sim 40 - 150$  fs time and  $\sim 1$  nm spatial resolutions. Ultrashort laser pulse transforms a frontal surface layer with thickness  $d_T$  into two-temperature ( $T_e \gg T_i$ ) warm dense matter state. Its quantitative characteristics including its thickness are defined by poorly known coefficients of electron-ion energy exchange  $\alpha$  and electron heat conductivity  $\kappa$ . Fast laser heating rises pressure in the  $d_T$ -layer and therefore produce acoustic waves. Propagation and reflection from the frontal and rear boundaries of these waves causes the displacement  $\Delta x(t)$  of boundary positions. Pressure wave profiles, and hence functions  $\Delta x(t)$ , depend on thickness  $d_T$ . This is why the experimental detection of  $\Delta x(t)$  opens a way to accurate evaluation of the coefficients  $\alpha$  and  $\kappa$ .

© 2010 WILEY-VCH Verlag GmbH & Co. KGaA, Weinheim

### 1 Introduction

Ultrashort laser pulse interaction with matter is an important part of modern technology and physics [1, 2]. Duration  $\tau_L$  of such pulses is shorter than a time  $t_{eq}$  of electron-ion energy transfer. Therefore, absorption of ultrashort pulse by electron subsystem leads to transition to two-temperature (2T) warm dense matter state (2T WDM). In the 2T WDM state electrons are much hotter than ions:  $T_e \gg T_i$  in condensed matter, because the main part of absorbed laser energy is in electron subsystem. The internal energy is about 1 eV per atom at the time  $t \sim t_{eq}$ . This value is typical in technological applications like surface microfabrication where removal of a material layer from target surface is required [1, 2]. This level of energy is of the order  $(0.2 - 0.4)E_{coh}$  of cohesion energy  $E_{coh}$  [3, 4], where  $E_{coh} \approx 3$  eV/atom for Al, Au, and Cu.

In 2T WDM state the electron thermal diffusivity  $\chi_e^{2T} = \kappa_e/c_{eV}$  is high in comparison with the room temperature (r.t.)

$$\chi_e^{1T}|_{r.t.} = \frac{\kappa_e + \kappa_i}{c_{eV} + c_i} \approx \frac{\kappa_e}{c_i} \approx 1 \text{ cm}^2 \text{ s}^{-1}, \quad \chi_e^{2T}(T_e = T_i, T_i = 300 \text{ K}) = \frac{\kappa_e}{c_{eV}} \approx 100 \text{ cm}^2 \text{ s}^{-1} \quad (\text{A1}),$$

\* Corresponding author: e-mail: [nailinogamov@googlemail.com](mailto:nailinogamov@googlemail.com), Phone: +07 495 425 8767, Fax: +07 495 702 9317

where "1T" means - one temperature  $T = T_e = T_i$ ,  $\kappa_e$  and  $\kappa_i$  are electron and phonon thermal conductivities,  $\kappa_e \gg \kappa_i$ ,  $c_{eV}|_{r.t.} \ll c_i \approx 3n_{at}k_B$ ,

$$\frac{c_{eV}(T_e)}{c_i} = 0.4T_{e,eV}, \quad \frac{E_e}{E_i} = 2.5\frac{T_{e,eV}^2}{T_{i,kK}}, \quad E_e = \frac{\gamma T_e^2}{2}, \quad E_i = c_i T_i, \quad (\text{Al}), \quad c_i \approx 3n_{at}k_B.$$

For our typical energy level the final temperature  $T = T_e = T_i$  of the heated layer is  $\sim 1.5$  kK. Corresponding energies are  $E_i/\rho \sim 0.4$  eV atom $^{-1}$ , electron temperature is  $T_e = 0.8$  eV, and the ratio of heat capacities is  $c_{eV}/c_i \approx 0.3$ . That  $\chi_e^{2T}$  is high as demonstrated by Fig. 1, [5]. Therefore, the absorbed heat penetrates deep into bulk of a target being in this state. Heat penetration depth  $d_T$  is in several times larger than light penetration depth  $d_{skin} \sim 10 - 20$  nm. This depth is called also thickness of skin-layer or extinction depth. Rough estimate is  $d_T \sim \sqrt{\chi t_{eq}}$ .

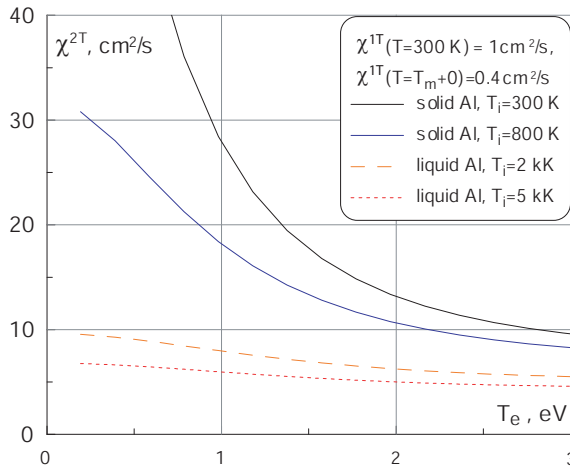


**Fig. 1** In 2T WDM state the electron heat diffusivity is high, because ions having large and temperature-independent heat capacity are only weakly thermally coupled with electrons for the time  $t < t_{eq}$  [5]. (Online colour: www.cpp-journal.org).

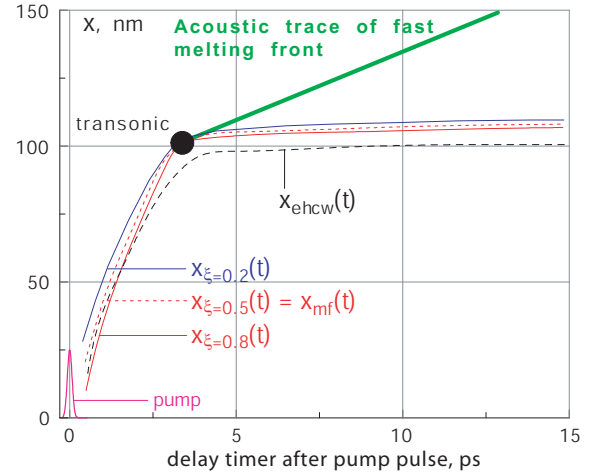


**Fig. 2** Layout of the trajectories of two-phase mixture fronts  $x_{mix0.2}$ ,  $x_{mix0.8}$ , the melting front  $x_{mf}$ , and the electron heat conduction wave  $x_{ehcw}$ . There are two-stages of the ion heating history: (a) short, 2T, supersonic and (b) long, 1T, subsonic. They are separated by the point "transonic". (Online colour: www.cpp-journal.org).

Due to high value of  $\chi$ , large thermal depth  $d_T$ , and short electron-to-ion energy transfer time  $t_{eq}$  the heating of material to a depth of  $d_T$  can be called supersonic. For fluences around ablation threshold the ion temperatures in the part of heated layer are significantly above melting temperature. Therefore, the fast non-equilibrium bulk melting takes place at 2T WDM state. Such melting also can be called supersonic, since it is supersonic in the sense that its phase velocity  $\sim d_T/t_{eq}$  is much higher than sound speed  $c_s$ . E.g. for Al  $c_s \approx 6$  km s $^{-1}$  while  $d_T/t_{eq} \approx 100\text{nm}/3\text{ps} = 30$  km s $^{-1}$ ,  $\dot{x}_{ehcw}(t) \sim 0.5\sqrt{\chi/t} \gg c_s$ , if  $t < t_{eq}$ . Thermal wave and melting front trajectories  $x_{ehcw}$  and  $x_{mf}$  are shown in Fig. 2. They are defined in reference to the point, where  $T_e(x, t)$  is a half of its instant maximum value, and an instant volume fraction of molten phase  $\xi$  in the solid-liquid mixture is 0.5.

It is clearly seen on Fig. 2 that there are supersonic 2T stage and subsonic 1T stage of heat penetration. For 2T stage the melting takes place through homogeneous volume nucleation, where a two-phase crystal-liquid transition layer around the melting front is wide. There is some delay time after ultrashort heating prior to appearance of melt [6]. In Fig. 2 the trajectories of two fronts limiting two-phase mixture are shown together with the melting front. They are defined at the points where liquid volume fraction  $\xi$  is equal to 0.2, 0.5, and 0.8 respectively. In the 1T stage the propagation of thermal wave is slow (subsonic), the melting continues due to heterogenous nucleation at the melting front, and the two-phase mixture zone becomes narrow. This observation about fast and slow stages of heat penetration agrees with works [7, 8]. At a late time ( $\sim 0.1 - 1$  ns) a molten layer starts to solidify from a depth of target, but not from frontal surface.

Supersonic propagations means that heating at 2T stage is fast enough to be called as isochoric heating. The material does not have time to expand which results in so-called stress confinement. Supersonic heat penetration

loads substance since pressure increases together with increase of internal energy, while specific volume remains as for a room temperature crystal.

The loaded layer releases later at the acoustic 1T stage. All subsequent dynamics is consequence of this release.

The unload of stress confinement zone creates powerful pressure disturbances traveling in a foil. Their reflection from frontal and rear-side boundaries induces boundary motion  $\Delta x(t)$  which can be experimentally detected by pump-probe technique. The obtained data are used to retrieve the acoustic profiles:  $\Delta x(t) \rightarrow p(x, t = t_{eq})$ . Hence, we can obtain data concerning creation of these profiles at the supersonic stage, which depends on the 2T parameters still poorly known for noble and transition metals. The present work is aimed to (a) simulation of 2T relaxation, acoustic interplay, reflection from boundaries, and (b) experimental measurements of time dependent displacements  $\Delta x(t)$ .

## 2 Acoustic traces of supersonic melting

There are two sonic traces of fast heating and melting. The first of them is connected with differences in the Gruneisen constant in crystal, crystal-liquid mixture, and molten metal. This is shown in Fig. 3, 4. Due to these differences the phase composition profile at the time  $t \approx t_{eq}$  "imprints" itself into the pressure profile of the acoustic compression wave. After that the acoustic wave keeps for a long time this imprinting (or in other words the trace of fast melting) during its traveling through a film. The imprinting is formed near the point "transonic" where the melting front decelerates from supersonic to subsonic velocity. In this space-time point the imprinting separates the from melting front and moves further with constant velocity equal to  $c_s$ . This is shown in Fig. 2 as the straight line beginning from the point "transonic".

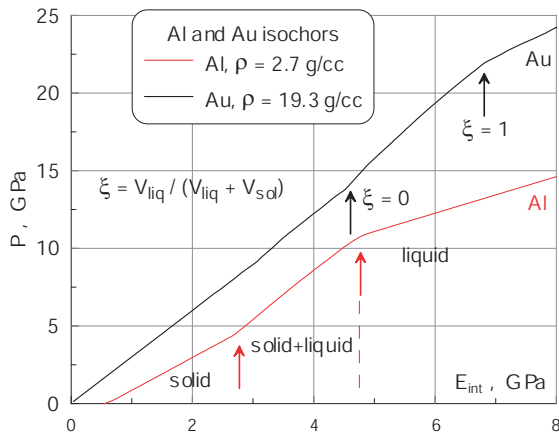


**Fig. 3** Changes in Gruneisen parameter as result of phase transition. The dependencies are plotted according to wide range equation of state [9]. (Online colour: www.cpp-journal.org).

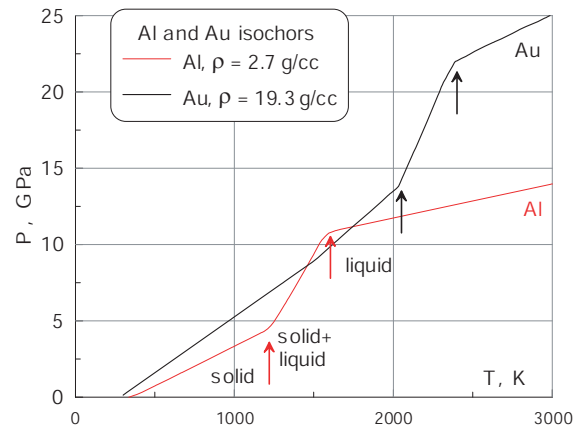


**Fig. 4** The kinks in the  $p(T)$  dependencies due to beginning and end of melting. (Online colour: www.cpp-journal.org).

Our experimental set up includes a glass plate 150 microns thick with an Al solid film deposited onto glass. Thickness of a film in experiments is different. It is varied from 0.4 to 1.5 microns. A pump laser pulse comes through transparent glass and is absorbed in Al extinction depth near glass-Al boundary.

Simulation results are shown in Figs. 5-7. The molecular dynamics (MD) code is described in [10]. The new EAM potentials used for MD simulation are presented in [3]. The 2T hydrodynamics (2T HD) is described in [6]. At 2T WDM state  $t < t_{eq} \approx 3$  ps movement of melting zone, located between liquid volume fractions  $\xi = 0$  and  $\xi = 1$ , is supersonic. The arrow "1-2" in Fig. 5 shows the shift of the melting zone with solid-liquid mixture during the time interval from  $t = 1$  ps to  $t = 2$  ps. Velocity of shift at this time interval is  $25 \text{ km s}^{-1}$ . At later times  $t > t_{eq}$  the imprint of melting propagates with sonic velocity  $c_s$ .

The kinks at the pressure profiles initially appears in connection with solid-liquid mixture zone, see the profiles  $t = 1$  and  $t = 2$  in Fig. 5. After appearance they live long life moving together with the traveling to the right acoustic compression wave, compare Figs. 5 and 6. At the 2T stage the kinks are pushed into bulk by supersonic electron heat transport. At this stage the kinks in the liquid volume fraction  $\xi$  and at the pressure profile are

linked to each other. While after sharp deceleration of electron heat transport the kinks in the pressure profile separate from the kinks in the profile of  $\xi$ . At the acoustic propagation stage the slope between kinks at the acoustic profile gradually becomes steeper and steeper. Transformation to a shock jump takes place if a foil is thick enough. Thus high Gruneisen value in solid-liquid mixture shown in Fig. 3 and fast melting increase the slope and hence enhance breaking of compression wave. The breaking is connected with nonlinearity ( $c_s$  is not constant but depends on pressure). The nonlinearity causes focusing and intersections of acoustic characteristics.

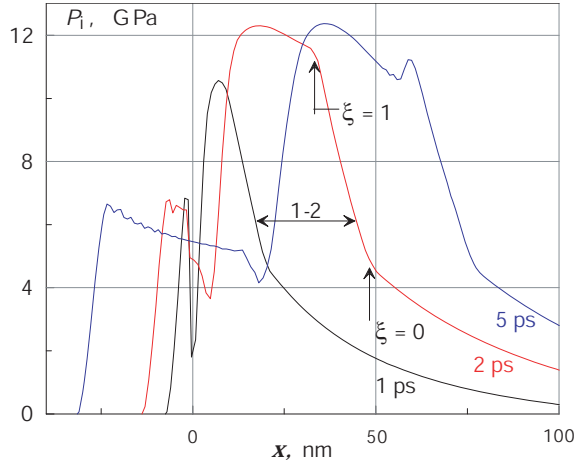


**Fig. 5** Propagation of lower and upper kinks at pressure profiles. The point  $x = 0$  initially separates glass and Al. For the profiles  $t = 1$  and  $t = 2$  ps these kinks are connected with the solid-liquid mixture zone. The beginning and the end of the mixture zone are marked by arrows  $\xi = 0$  and  $\xi = 1$ , compare with the similar arrows in Fig. 3. At  $t \approx t_{eq} \approx 3$  ps the kinks separate from the decelerating electron heat wave and the solid-liquid mixture zone and propagate further through solid metal as the acoustic wave. (Online colour: [www.cpp-journal.org](http://www.cpp-journal.org)).

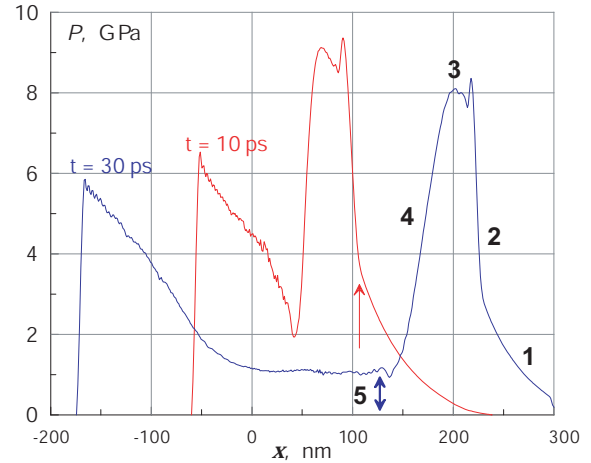


**Fig. 6** Evolution of the compression wave with the kinks. It moves to the right from the glass-Al boundary  $x = 0$ . The kinks are traces of supersonic melting. The five elements constituting the pressure profile are labeled from (i) to (v). All five of these elements appears also in the  $\Delta x(t), v(t)$  profiles of displacements of the rear-side boundary if the film is thin enough. In the thicker films the element (i) disappears as it is absorbed by the lower kink. (Online colour: [www.cpp-journal.org](http://www.cpp-journal.org)).

The profile of compression wave moving to the right consists from five elements, see Fig. 6.

(1) There is the precursor before the lower kink. It corresponds to the tail of the 2T fast electronic heating wave. Gradually it becomes weaker as the moving faster lower kink absorbs it.

(2) There is the described above steep increase of pressure between the kinks. At the rear-side of the thick film this increase looks like a jump.

(3) There is the head of the profile behind the upper kink. It depends on the value of the Gruneisen number in melt and on the electron heat conductivity coefficient  $\kappa$  at the 2T stage. The  $\kappa^{liq}$  is smaller than the  $\kappa^{sol}$ . Therefore at the 2T stage the electron temperature gradient is steeper in the melt. After formation of the right shock thickness of the head gradually becomes smaller because behind the shock the flow is subsonic. The maximum pressure at the head (3) becomes smaller than the value of pressure at the upper kink in Figs. 3 and 4 due to slow decay of the jump (2) connected with nonlinear acoustics. The length of the head (3) also becomes shorter.

(4) There is the decrease of pressure in the rarefaction wave shown as the right arrow  $c_s t$  in Fig. 7.

(5) feature is important because it is a plateau behind the rarefaction wave. The plateau is marked by the thick vertical two side arrow shown in 6 at the profile corresponding to  $t = 30$  ps.

The compression wave propagating to the left with a shock ahead differs from the right compression wave due to the supersonic processes at the 2T stage and due to nonlinearity. In linear acoustic, valid for smaller values of absorbed fluence  $F_{abs}$ , these left and right waves are equal.

The plateau (5) in Fig. 6 is the second acoustic trace of the fast heating and melting. This trace appears due to rather long expansion of  $d_T$  thick heated and molten layer of Al confined between glass and cold solid Al. This is shown in Figs. 8-12. The plateau is connected with reflection of the compression wave going to the left into

glass from the glass-Al boundary. The pressure amplitude of the plateau depends on temperature of the  $d_T$ -layer after 2T relaxation: if this temperature is higher than the plateau is higher. The hot  $d_T$ -layer (the entropy layer) remains near glass-Al boundary after separation of acoustic waves from it. Adiabatic expansion slightly reduces its temperature. At late time effect of heat conduction is small therefore for this time interval the flow may be described as adiabatic flow.

All laser heat is absorbed in an extinction depth of Al. Glass is heated weakly by the shock moving to the left, see Figs. 11 and 12. The pressure jump created supersonically by the pump pulse at the  $x = 0$  glass-Al boundary decays into the shock moving into glass and into the rarefaction wave moving to the right. They are marked by the left and right arrows  $c_s t$  in Fig. 7.

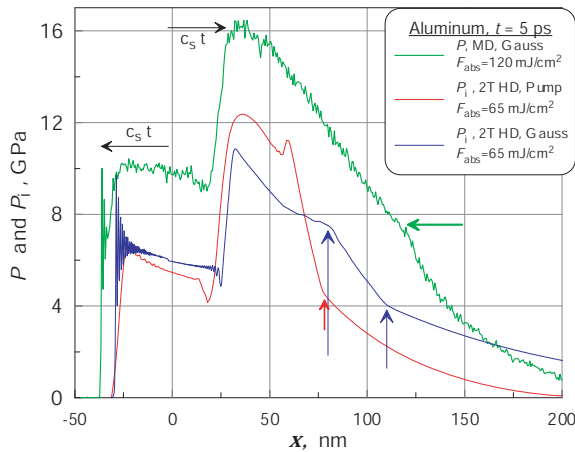


**Fig. 7** Creation of peculiarity at pressure profile due to fast melting is universal. Here different simulations are compared. The 2T HD codes use equilibrium equation of state with equilibrium melting. While the MD code reproduces real kinetics of melting. (Online colour: www.cpp-journal.org).

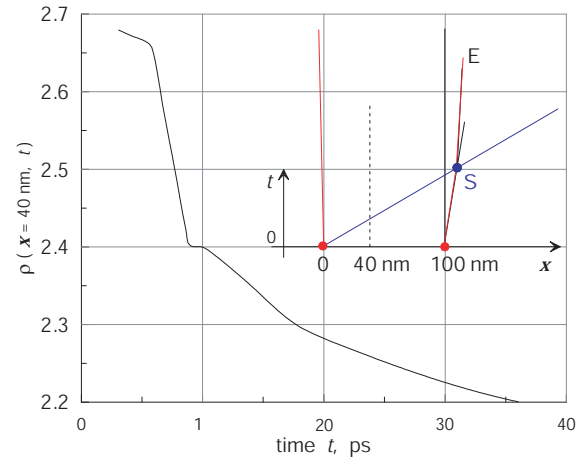


**Fig. 8** Decrease of density in the  $d_T$ -layer as result of volume expansion of heated matter (solid black curve). In this example density is taken in the point  $x = 40$  nm inside the  $d_T$ -layer from the MD simulation shown in Fig. 7. This point is given as dashed straight vertical line in the inset representing the  $x, t$ -diagram. See details in text. (Online colour: www.cpp-journal.org).

In the inset in Fig. 8 the left line, starting from the point  $x = 0$ , is the boundary between glass and Al. It slowly moves to the left side since Al is heated and expands. The right vertical straight line is the line  $x \equiv 100$  nm. The point  $x = 100$  nm corresponds to the position of the right boundary of the heated layer  $d_T$  when temperatures  $T_e$  and  $T_i$  equilibrates. The vertical line  $x \equiv 100$  nm is drawn to emphasize expansion of the heated layer to the right side. The left and right boundaries of the  $d_T$ -layer are shown by red lines.

In linear acoustics the expansion of the right boundary of the  $d_T$ -layer stops in the point S when the characteristic ( $x = 0$ )-S, going from the point  $x = 0$  to the point S, intersects this boundary (sharp end of expansion). The characteristic ( $x = 0$ )-S is shown by blue line. In our case the expansion continues after this intersection. This is the result of deviation from linear acoustics.

Therefore, firstly, the density  $\rho(x = 40 \text{ nm}, t)$  continues to decrease after the instant  $t = 7$  ps defined in the next lines. The time dependence  $\rho(x = 40 \text{ nm}, t)$  is given by the black continuous curve in Fig. 8. Secondly, the line S-E in the inset continues to move to the right. The line S-E is the right boundary of the  $d_T$ -layer. This is the continuation of the expansion of the  $d_T$ -layer after the intersection S.

The event at the instant  $t = 7$  ps at the curve  $\rho(x = 40 \text{ nm}, t)$  corresponds to arrival of the characteristic ( $x = 0$ )-S to the point  $x = 40$  nm;  $40 \text{ nm}/c_s \approx 7$  ps. This is the intersection of the dashed vertical straight line in the inset and the characteristic. Expansion is driven by the temperature difference inside and outside the  $d_T$ -layer and melting, since density of liquid Al is smaller than density of solid under the same pressure.

There are two acoustic stages (linear and nonlinear) of expansion of the  $d_T$ -layer of high entropy, see Fig. 9. The second stage exists as result of nonlinearity. Non-linear effect is appreciable since the amplitude of the relative density perturbation  $\delta\rho/\rho^o$  in the  $d_T$  entropy layer is not very small. This amplitude is  $\approx 20\%$ . The

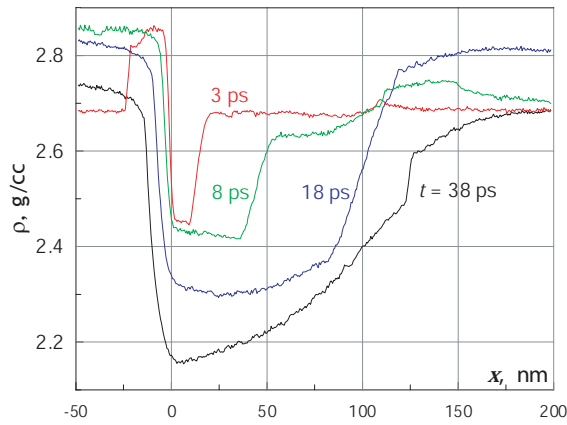


**Fig. 9** Two stages of volume expansion of the  $d_T$ -layer. The first (linear acoustic) stage finishes when the characteristic  $x = 0$ -S shown in the inset in Fig. 8 intersects in the point S  $t = 17$  ps the right boundary of the  $d_T$  layer. After that expansion continues at the nonlinear acoustic stage - compare profiles for  $t = 18$  ps and  $t = 38$  ps. (Online colour: www.cpp-journal.org).

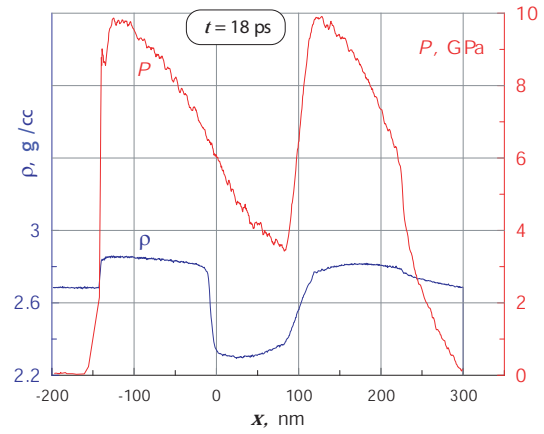


**Fig. 10** Creation of the density well connected with the entropy layer and separation of the left and right compression waves from the entropy layer (MD simulation). The left jump is the shock in the glass. The right density drop is the rear-side boundary of the Al film 300 nm thick. (Online colour: www.cpp-journal.org).

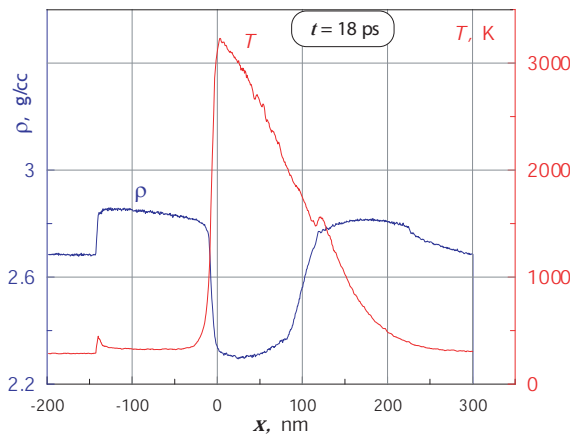


**Fig. 11** The coincidence between the density well and the entropy layer. The density well is established gradually during the two acoustic stages. (Online colour: www.cpp-journal.org).

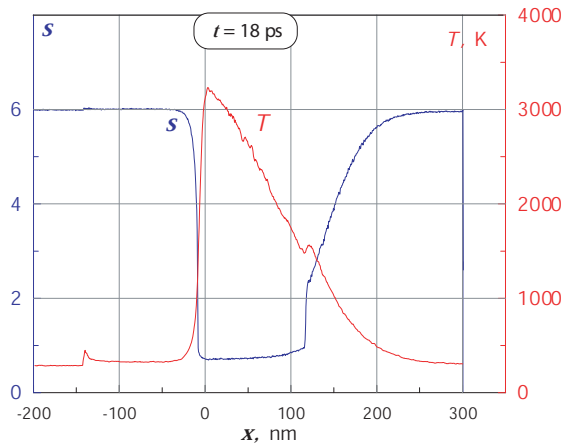


**Fig. 12** The coincidence between the molten and the entropy layers in case of  $F_{abs} = 120$  mJ/cm<sup>2</sup> absorbed in Al. (Online colour: www.cpp-journal.org).

second stage corresponds to the tail of slow expansion at the interval  $\approx 8$  ps  $< t < 36$  ps in Fig. 8. It is slow in comparison with expansion at the interval  $\approx 6$  ps  $< t < 8$  ps in Fig. 8.

As was said above, in linear acoustics the expansion will stop when the characteristic ( $x = 0$ )-S leaves the  $d_T$ -layer. In the case of linear acoustics the density decrease in the  $d_T$ -layer finishes at the instant  $t \approx 17$  ps corresponding to the point S in the inset in Fig. 8. In the non-linear case the decrease of density continues - compare profiles for  $t = 18$  ps and  $t = 38$  ps in Fig. 9. Expansion at the non-linear stage supports the pressure tail (5) of the compression wave shown in Fig. 6.

Creation of the density well shown in Figs. 9-11 continues during linear and nonlinear acoustic stages as was explained in Fig. 9. The high temperature distribution inside the  $d_T$  layer is established during the short 2T stage. The 2T stage is short in comparison with the acoustic scale of time  $d_T/c_s$ . This establishment takes place before the hydrodynamic motion begins and density is disturbed. During the two acoustic stages temperature slightly decreases due to losses spent to adiabatic expansion.

Figures 10 and 11 illustrate that the pressure profiles of the compression waves separate from the temperature distribution and begin independent propagation. While initially the temperature and the pressure profiles were closely tied - as isochoric heating rises pressure. Later, as it was said, the pressure disturbance moves away, but the temperature profile remains frozen into matter, see Figs. 10-12. Indeed, the pressure profile after short 2T stage is similar to the "triangular" temperature profile in Fig. 11. After that the pressure profile splits to two (left and right) "triangular" compression waves propagating to the left and to the right sides. They are shown in Fig. 10.

Molten Al remains under significant pressure (see Fig. 10) at the instant shown in Fig. 12. Therefore temperature at the melting front is higher than the triple point temperature in Al (934 K), and density of liquid is higher than density at the binodal (the vapor-liquid coexistence curve) in the triple point. Position of the melting front is defined by the profile of the symmetry index  $s$ .  $s$  is a measure of local order. It is calculated for every atom. In Fig. 12 the profile  $s(x, t)$  is shown. It is obtained by averaging over atoms.  $s$  for the fixed atom is equal to a number of axis (a) passing through this atom and (b) having two neighbor atoms opposite to each other relative to the fixed atom [6].

Pure liquid begins when the symmetry index  $s$  drops below the value  $s = 2.2$ . Position of the melting front is connected also with the small peculiarity at the temperature profile in Fig. 12. There is also a transition zone covering range  $2.2 < s < 6$  with hot deformed crystal. The value  $s = 6$  corresponds to an ideal fcc Al crystal.

### 3 Movement of rear-side boundary

Dynamics of the rear-side boundary is shown in Figs. 13 and 14. In these measurements the titan-sapphire laser with the pump 800 nm and the probe 400 nm pulses and enlarged duration 150 fs is used (usual duration is 40 fs). The duration was enlarged to increase threshold fluence  $F_{ob}$  of an optical breakdown in glass and thus (see below) increase pressure in Al. The scheme of laser light propagation through glass is shown in the inset in Fig. 13.

Number of experiments with different pump incident fluences  $F_{inc}$  have been carried out. It was important to achieve significant pressure  $p(F_{abs})$  in Al. Function  $p(F_{abs})$  grows with fluence absorbed in Al. Values  $F_{abs}(F_{inc})$  increase with  $F_{inc}$  and saturates when  $F_{inc}$  reaches the threshold  $F_{ob}$ . Further increase of  $F_{inc}$  does not increase  $F_{abs}$  and  $p$ , since the excess of  $F_{inc}$  above the threshold  $F_{ob}$  is absorbed in glass. It is clear that in the case with higher  $F_{ob}$  the "saturated" pressure is higher.

In Figs. 13 and 14 the instant  $t = 0$  is the maximum of the pump pulse for the 2T HD curves, see Fig. 2. The experimental data is not synchronized relative to the pump maximum. Therefore in Fig. 13 the markers were shifted along the axis of delay time to obtain the best fit. The points  $\Delta x_{rear} = 0$  and  $v_{rear} = 0$  correspond to the initial position of the rear-side boundary.

The precursor (1) in Figs. 13 and 14 is weak. The experiment did not find it. Thinner films are necessary to investigate the precursor. The experimental and simulated jump amplitudes (2) are in agreement. The amplitude of the maximum velocity (3) and the position in time of this maximum agree well. The rarefaction (4) also is well described. The plateau (5) is clearly pronounced in the experimental data. This means that indeed long and powerful expansion of quickly molten Al takes place.

### 4 Conclusion

Ultrashort laser pulse produces thermomechanical loading and pressure waves. It also triggers supersonic melting which interferes with these waves. This acoustic interference causes (a) premature breaking of compression wave with formation of shock, and (b) appearance of the long tail with positive pressure behind the compression wave. It is shown in the paper, that this long tail exists in the experimentally measured time-dependence of the rear-side shift  $x_{rear}(t)$ . Coincidence between experimental and theoretical functions  $x_{rear}(t)$  means that physical model [5, 6] correctly predicts amplitude and width of the main pressure wave and the tail behind it. This means also that the model describes two-temperature details, since the amplitude, width, and tail depend on these details.

**Acknowledgements** Work of MBA, SIA, NAI, VVZh, VAK, and YuVP has been supported by the RFBR grant No. 09-08-00969-a.

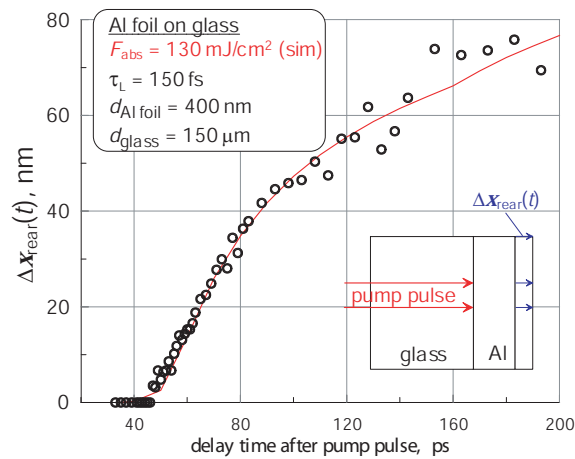


**Fig. 13** Experimental (circles) and simulation (solid line, 2T HD) results. The inset presents the irradiation conditions: the pump heats Al through glass plate, and the sequence of the probe pulses measures the time-dependent shifts of the rear surface. (Online colour: [www.cpp-journal.org](http://www.cpp-journal.org)).

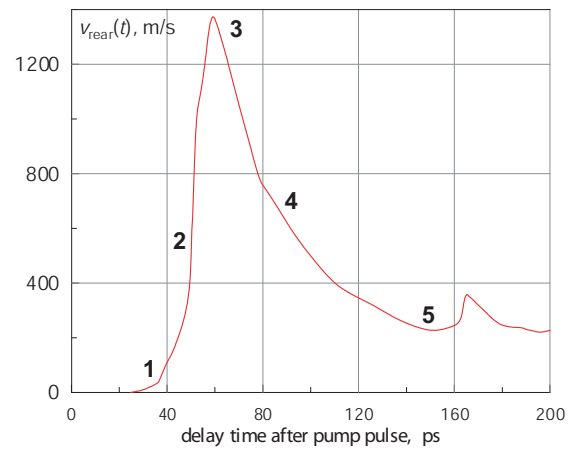


**Fig. 14** The velocity profile  $v_{rear}(t)$  contains information about the shape of the pressure profile. Compare the five elements (1)-(5) here and in Fig. 6. Agreement between experimental and simulated data in Fig. 13 allows to say that the coefficients  $\alpha, \kappa$  [5] used in the 2T physical model are correct. (Online colour: [www.cpp-journal.org](http://www.cpp-journal.org)).

## References

- [1] C. Phipps, (Ed.) "Laser Ablation and its Applications", Springer Series in Optical Sciences, Volume 129 (2007).
- [2] A. I. Kuznetsov, J. Koch, B. N. Chichkov. *Appl. Phys. A*, **94**, 221 (2009).
- [3] V. V. Zhakhovskii, N. A. Inogamov et al. *Appl. Surf. Sci.*, **255**, 9592 (2009).
- [4] A. K. Upadhyay, N. A. Inogamov, B. Rethfeld, H. M. Urbassek. *Phys. Rev. B*, **78**, 045437 (2008).
- [5] N. A. Inogamov, Yu. V. Petrov. *JETP*, **137**, No. 2 (2010). In press.
- [6] N. A. Inogamov, V. V. Zhakhovskii, S. I. Ashitkov et al. *Appl. Surf. Sci.*, **255**, 9712 (2009).
- [7] D. A. Thomas, Z. Lin, L. V. Zhigilei, E. L. Gurevich, S. Kittel, R. Hergenroeder. *Appl. Surf. Sci.*, **255**, 9605 (2009).
- [8] Wai-Lun Chan, R. S. Averback, D. G. Cahill, A. Lagoutchev, *Phys. Rev. B*, **78**, 214107 (2008).
- [9] A. V. Bushman, G. I. Kanel', A. L. Ni, V. E. Fortov, *Intense dynamic loading of condensed matter*, Taylor & Francis Translation., 295 p. (1993).
- [10] V. V. Zhakhovskii et al., *IEEE Proceeding of the 5th International Symposium on Cluster Computing and Grid*, **2**, 848 (2005).